Closure of the meridional overturning circulation through Southern Ocean upwelling

John Marshall[1]* and Kevin Speer[2]

The meridional overturning circulation of the ocean plays a central role in climate and climate variability by storing and transporting heat, fresh water and carbon around the globe. Historically, the focus of research has been on the North Atlantic Basin, a primary site where water sinks from the surface to depth, triggered by loss of heat, and therefore buoyancy, to the atmosphere. A key part of the overturning puzzle, however, is the return path from the interior ocean to the surface through upwelling in the Southern Ocean. This return path is largely driven by winds. It has become clear over the past few years that the importance of Southern Ocean upwelling for our understanding of climate rivals that of North Atlantic downwelling, because it controls the rate at which ocean reservoirs of heat and carbon communicate with the surface.

A conceptual model of the meridional overturning circulation (MOC) of the ocean is that of the filling box[1,2]. The box represents the ocean basin. The filling process is the conversion in polar oceans of light upper water to denser deep water by convection and mixing in the open seas and in shelf and bottom boundary-layer processes[3]. These dense waters rise in the basins and ultimately, after a circuitous route that we discuss here, flow back towards the sinking regions to close the circulation meridionally. As sketched schematically in Fig. 1, two meridional overturning cells emanate from polar formation regions: an upper cell associated with sinking to mid-depth in the northern North Atlantic and a lower cell associated with sources of abyssal water around Antarctica. Although the polar source regions for these overturning cells have been identified, detailed upwelling pathways back to the surface and the underlying controlling physical mechanisms have long been debated, but they have now come into clearer focus.

The main theme of this Review is the key role of Southern Ocean upwelling driven by westerly winds, drawing water up to the surface. This largely solves the missing-mixing paradox that has remained a theme of oceanographic literature[4,5]. In that paradox, all dense water was assumed to upwell through the thermocline to close the circulation. To do so, strong vertical mixing is required in the thermocline, mixing that is not observed[6–9]. Instead it seems that a significant portion of the water made dense in sinking regions ultimately returns to the surface in nearly adiabatic pathways along tilted density surfaces that rise from depth towards the surface around Antarctica (as hypothesized long ago by Sverdrup[10]). These tilted surfaces mark the great density difference between the subtropics and polar regions associated with the planet's largest current, the Antarctic Circumpolar Current (ACC). They connect the interior ocean to the sea surface enabling fluid that has sunk to depth at high latitudes to return to the surface without the need to invoke large thermocline diffusivities. Recent modelling and theoretical studies point to a global influence on climate of this upwelling branch[11–14]. We conclude our Review with an updated schematic of the global overturning circulation that makes explicit the central role of Southern Ocean upwelling.

Observations of Southern Ocean circulation

Key climatological features of the circulation and hydrography of the Southern Ocean are shown in Fig. 2. The circulation is dominated by the eastward-flowing, vigorously eddying ACC. The ACC has a braided flow structure with embedded regions of strong fronts, of which the subantarctic and polar fronts are the most pronounced. The fronts show evidence of topographic steering, often being collocated with gaps in the topography. The polar front roughly marks the northern boundary of sea-ice influence, but ice concentration is very low approaching the ACC. South of the polar front, sea ice grows and decays seasonally (as does light), with large consequences for ocean physics and biology. Hydrographic sections of temperature (T), salinity (S) and oxygen (O_2) are shown along a longtitude of 30° E, crossing the ACC from Africa to Antarctica. Property horizons rise southwards, following tilted surfaces of constant density associated with the thermal wind balance of the ACC. The distribution of salinity shows the freshening to the south at the surface, the spreading of low-salinity surface water along isopycnals in Antarctic Intermediate Water, and high salinity values at mid-depth owing to the influence of salty North Atlantic Deep Water (NADW). Oxygen concentration shows high values at the surface, decreasing to the mid-depth minimum of Upper Circumpolar Deep Water—essentially older deep water, which also aligns with the climatically important subsurface temperature maximum. This pattern, revealed by many other tracers, has long been suggestive of a two-cell MOC (as sketched in Fig. 1) with incoming deep, relatively warm, salty, oxygen-depleted, carbon-rich and nutrient-rich water feeding an upper and lower cell.

A number of attempts have been made to infer the pattern of MOC in the Southern Ocean from tracer observations such as those summarized in Fig. 2. Among the first to observe and make use of salinity and other property distributions, Deacon[15] sketched a southward deep flow and northward shallow flow across the ACC. Earlier, Sverdrup[10] had proposed a broad circumpolar cross-ACC flow or overturning, which was quantified in a conceptual model by Wyrtki[16], linking the observed density and wind fields to infer southward ageostrophic flow and upwelling. Subsequent studies elaborated on the large-scale circulation in the Southern Ocean and

[1]Department of Earth, Atmospheric and Planetary Sciences, Massachusetts Institute of Technology, Building 54, Room 1520, Cambridge, Massachusetts 02139-4307, USA, [2]Department of Oceanography, Florida State University, Room 431A OSB, Tallahassee, Florida 32306-4320, USA.
*e-mail: jmarsh@mit.edu.
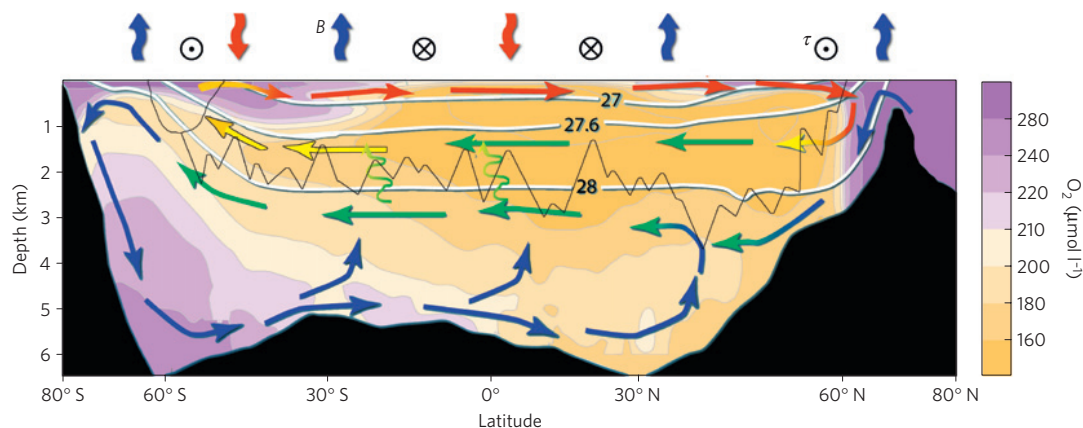
Figure 1 | A schematic diagram of the Upper Cell and Lower Cell of the global MOC emanating from, respectively, northern and southern polar seas. The zonally averaged oxygen distribution is superimposed, yellows indicating low values and hence older water, and purples indicating high values and hence recently ventilated water. The density surface 27.6 kg m^{-3} is the rough divide between the two cells (neutral density is plotted). The jagged thin black line indicates roughly the depth of the Mid-Atlantic Ridge and the Scotia Ridge (just downstream of Drake Passage) in the Southern Ocean (see Fig. 2). Low-latitude, wind-driven shallow cells are not indicated. General patterns of air–sea surface density (equivalent buoyancy) flux, *B* (red or blue indicating that surface waters are being made less or more dense, respectively; broad pattern of zonal surface wind stress, **τ**, ⊙: eastward; ⊗, westward). Coloured arrows schematically indicate the relative density of water masses: lighter mode and thermocline waters (red), upper deep waters (yellow), deep waters including NADW (green) and bottom waters (blue). Mixing processes associated with topography are indicated by the vertical squiggly arrows. This schematic is a highly simplified representation of a three-dimensional flow illustrated more completely in Box 1.

exchanges with other basins through descriptions of water-mass distributions[17–19] and major fronts[20–22].

More recently, inverse methods have been used to provide basin-scale estimates of mass and property transport by exploiting basic conservation principles applied over boxes, such as those delineated by the hydrographic sections shown in Fig. 2a, and assumptions about the statistics of property distribution[23–25]. Zonal average estimates have also been deduced from air–sea fluxes[26] and from observations of surface winds and surface currents, making use of residual mean theory[27,28]. Tracer observations have been exploited in greater detail to determine the explicit dependence of Southern Ocean overturning on mixing coefficients[29], generally showing that low diapycnal mixing is consistent with plausible circulation patterns and strengths. Many details are uncertain as data are relatively sparse, the circulation is not well known close to the continent within the ice pack[30], and the air–sea fluxes that force the ocean remain poorly constrained by observations and models. Nevertheless, certain robust features of the circulation emerge, as we now describe.

The inversion of Lumpkin and Speer[25] (see Fig. 3) shows that two global scale counter-rotating meridional cells dominate the overturning circulation and represent distinct circulation regimes, much as schematized in Fig. 1. The upper cell is fed both from the northern Atlantic, where buoyancy loss triggers convection and sinking in the marginal seas (forming various components of NADW) and also from below by deep diapycnal upwelling. The convergence of flow at intermediate depths is roughly balanced by upwelling in the Southern Ocean, induced by the strong, persistent westerly winds that blow over it (Fig. 4a). Surface buoyancy fluxes associated with fresh water and heat gain[31,32] (Fig. 4b), convert upwelling water to less dense Subantarctic Mode Water. In contrast, the lower cell is fed by dense-water formation processes around Antarctica, principally in the Ross and Weddell seas, forming Antarctic Bottom Water; it is the result of a balance between buoyancy loss by air–sea fluxes (Fig. 4b) and sea-ice export (Fig. 4c) around Antarctica and buoyancy gain by abyssal mixing. Only the overall transports are represented in Fig. 3; the inversion is independent of the detailed mechanisms that control the fluxes of mass into and out of upwelling or sinking regions.

The 27.6 kg m^{-3} density surface, outcropping south of the polar front all the way around Antarctica (see the white line in Fig. 4a,b),

marks the average division between the upper and lower cells in the Southern Ocean, as indicated in the schematic in Fig. 1 and the dotted line in Fig. 3b. Water crossing ~30° S in the Atlantic roughly in the range of 27–27.6 kg m^{-3} enters the Southern Ocean and rises up to the surface where it is exposed to surface buoyancy gain (Fig. 4b) and northward Ekman transport induced by the westerly winds: see the zonal wind stress in Fig. 4a and the consistently northward (Ekman) component of the surface currents driven by it evident in Fig. 2a. Waters entering the Southern Ocean from the Atlantic at densities greater than 27.6 kg m^{-3} upwell and outcrop near the Antarctic continent and are transformed into dense bottom water. About 75% of NADW enters the lower cell and is transformed to even denser bottom-water classes. Some becomes Antarctic Bottom Water. The remainder enters the Indian and Pacific oceans as Circumpolar Deep Water where abyssal mixing transforms it to lighter water ($\lesssim 27.6$ kg m^{-3}). It then re-enters the upper cell returning again southwards and upwards to the surface.

Is the return flow to the surface in the Southern Ocean enabled by interior mixing? Note that the abyssal ocean is stratified, albeit weakly so, and thus interior mixing must be acting here to vertically diffuse properties that are initially set by high-latitude processes and carried into the abyss by sinking fluid[5]. Such mixing is thought to occur primarily near topographic ridges, the tops of which are marked in Figs 1 and 3. This fundamentally diabatic part of the overturning circulation facilitates upward transfer of water in the lower cell to mid-depths in the world ocean basins (the blue to green transition in Fig. 1). Once water reaches mid-depths, however, the outcropping density field of the Southern Ocean provides a quasi-adiabatic route directly to the surface (green–yellow–orange in Fig. 1), feeding both the upper and lower cells of the MOC. Some inverse calculations indicate that important diabatic processes are at work even here in the upper cell[23]. A measure of mixing is indeed acting on the upwelling branch (note the gentle drift of the southward flow towards lighter densities in Fig. 3 above topography). However, it is generally thought that diapycnal mixing rates in the thermocline are small[9,25]. Notably, upwelling from depth directly through the thermocline, enabled by elevated levels of diapycnal mixing, is not observed. We now review what is known about the dynamical processes at work in the upwelling branch.
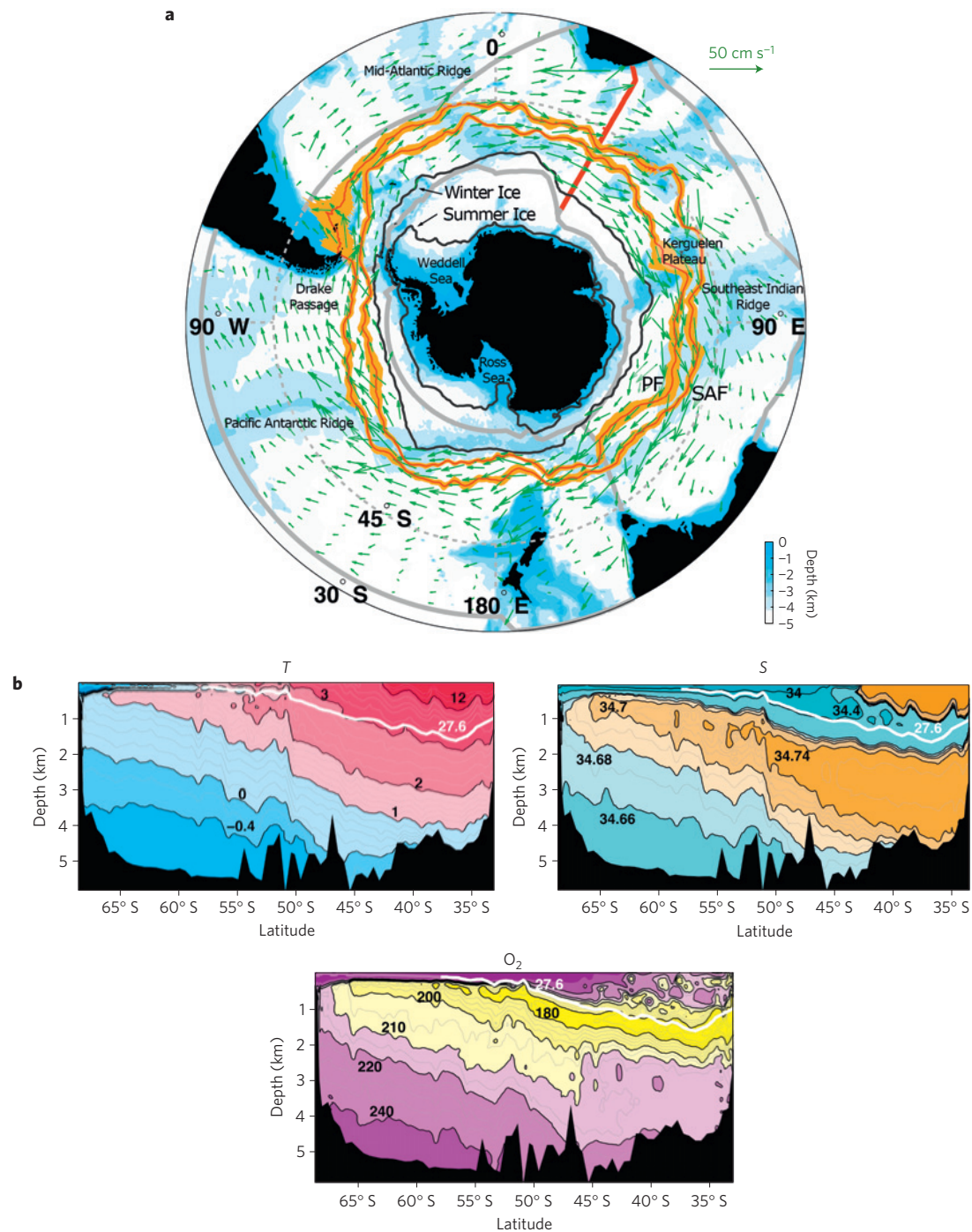
Figure 2 | Key observations in the Southern Ocean. a, Climatological positions of the subantarctic front (SAF) and polar front (PF) are marked in orange, with the thickness of the line representing the variance in the latitudinal position. The green arrows indicate the observed speed and direction of surface ocean currents as measured by drifters floating at a depth of 15 m (note the scale in the upper right-hand side). The depth of the ocean is colour coded in blue: the main topographic features are labelled. The black lines mark the summer (minimum) and winter (maximum) extent of sea ice. The position of key hydrographic sections are marked by the thick grey lines. **b**, *T* (temperature), *S* (salinity), and O_2 sections along 30° E (coloured red in **a**) cutting across the ACC from Africa towards Antarctica. Black contours are labelled in °C (for *T*), psu (for *S*) and μmol l^{-1} (for O_2). The thick white line is the 27.6 kg m^{-3} density surface.

Dynamics of the Southern Ocean and its upwelling branch

The Southern Ocean is driven by surface fluxes of momentum and density (owing to heat and fresh water) induced by the strong, predominantly westerly winds that blow over it and the freezing phenomena close to the continent[33]. Zonal wind stress (Fig. 4a) induces upwelling polewards of the zonal surface-wind maximum and downwelling equatorwards of the maximum. This directly wind-driven circulation, known as the Deacon cell, acts to overturn density surfaces supporting the thermal wind current of the ACC and creating a store of available potential energy.

Air–sea fluxes generate dense water near the continent and lighten the surface layers in the ACC (see Fig. 4b). The dense water sinks and tends to draw in warmer, saltier water from the surrounding ocean; however, rather than being fed from the surface,
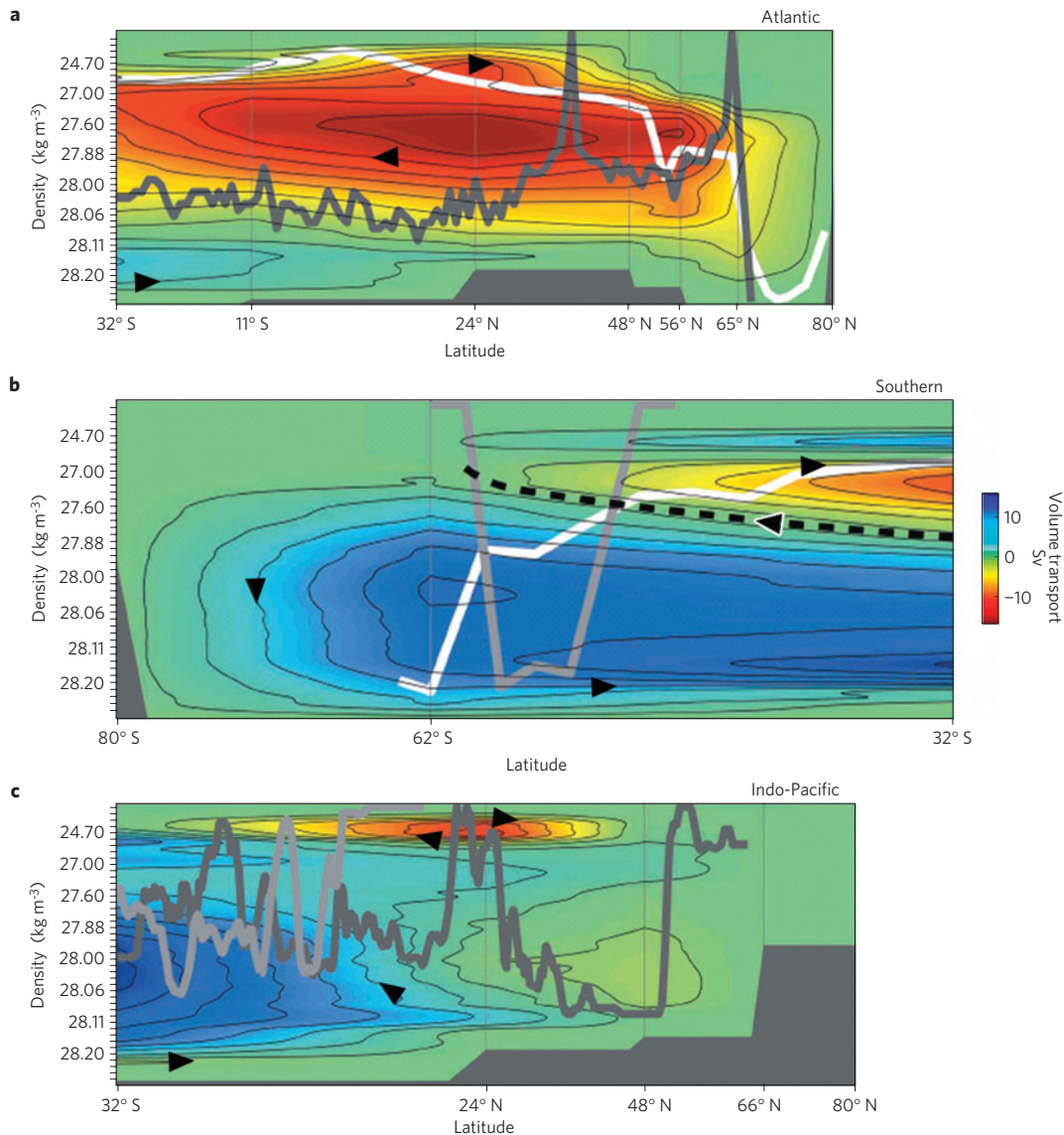
Figure 3 | Global MOC of the ocean obtained by tracer inversion a, Atlantic, **b**, Southern and **c**, Indo-Pacific oceans contoured every 2 Sv (1 Sv = 10^6 m^3 s^{-1}), plotted as a function of latitude and density. The dashed line in the Southern Ocean divides the upper and lower cells and roughly corresponds to (neutral) density surface 27.6 kg m^{-3}, which outcrops in the latitude range of Drake Passage, marked on Fig. 4. Grey lines indicate the crest of the Mid-Atlantic Ridge in the Atlantic and the main bathymetric features of the Pacific (dark) and Indian (light) ocean basins and the Scotia Ridge in the Southern Ocean. The thick white line represents the densest water modified by air–sea fluxes over the seasonal cycle. Modified from Lumpkin and Speer[25].

water is supplied from deeper layers along inclined outcropping density surfaces. Rising warmer deep water (clearly evident in Fig. 2b) melts ice both on the shelf and in the open ocean, controlling the northern extent of the cryosphere. This perhaps also accounts for the marked coincidence between the 27.6 kg m^{-3} outcrop (white line in Fig. 2a,b) and the winter ice edge (black line).

The overturning of density surfaces by winds is balanced, we believe, through the baroclinic instability of the thermal wind currents, an instability that acts to flatten out the density surfaces and to transport mass polewards. The resulting highly energetic, time-dependent eddying motions (analogous to atmospheric weather systems) have a scale of ~100 km and are a ubiquitous feature of the circumpolar flow. From an energetic perspective, much of the potential energy imparted to the ocean by the mechanical tilting of density surfaces is extracted by eddies flattening them out[34,35]. Indeed the Southern Ocean is a principal region where energy is imparted to the ocean by the wind[36] and it is here that we observe the most widespread mesoscale eddy field

in the ocean, extending all the way along the path of the ACC and throughout the depth of the water column.

Through their ability to transport mass, heat and potential vorticity (related to angular momentum) across the mean axis of the ACC, eddies are key to understanding the dynamics of the ACC (refs 35,37–43). Indeed, the clockwise-flowing upper meridional cell in the Southern Ocean is part of a residual circulation in which lateral eddy fluxes largely balance the wind-driven circulation[35,44]. This can be shown by decomposing the mass transport in a density layer of thickness h into mean and eddy contributions to define what is known as the residual flow:

$$\overline{vh} = \underbrace{\bar{v}\bar{h}}_{\substack{\text{mean transport} \\ \bar{\psi}}} + \underbrace{\overline{v'h'}}_{\substack{\text{eddy transport} \\ \psi^*}} = \underbrace{v_{\text{res}}\bar{h}}_{\substack{\text{residual transport} \\ \psi_{\text{res}}}} \qquad (1)$$

Here the meridional velocity is $v = \bar{v} + v'$, and so on, where the overbar denotes a time and streamwise average and primes denote
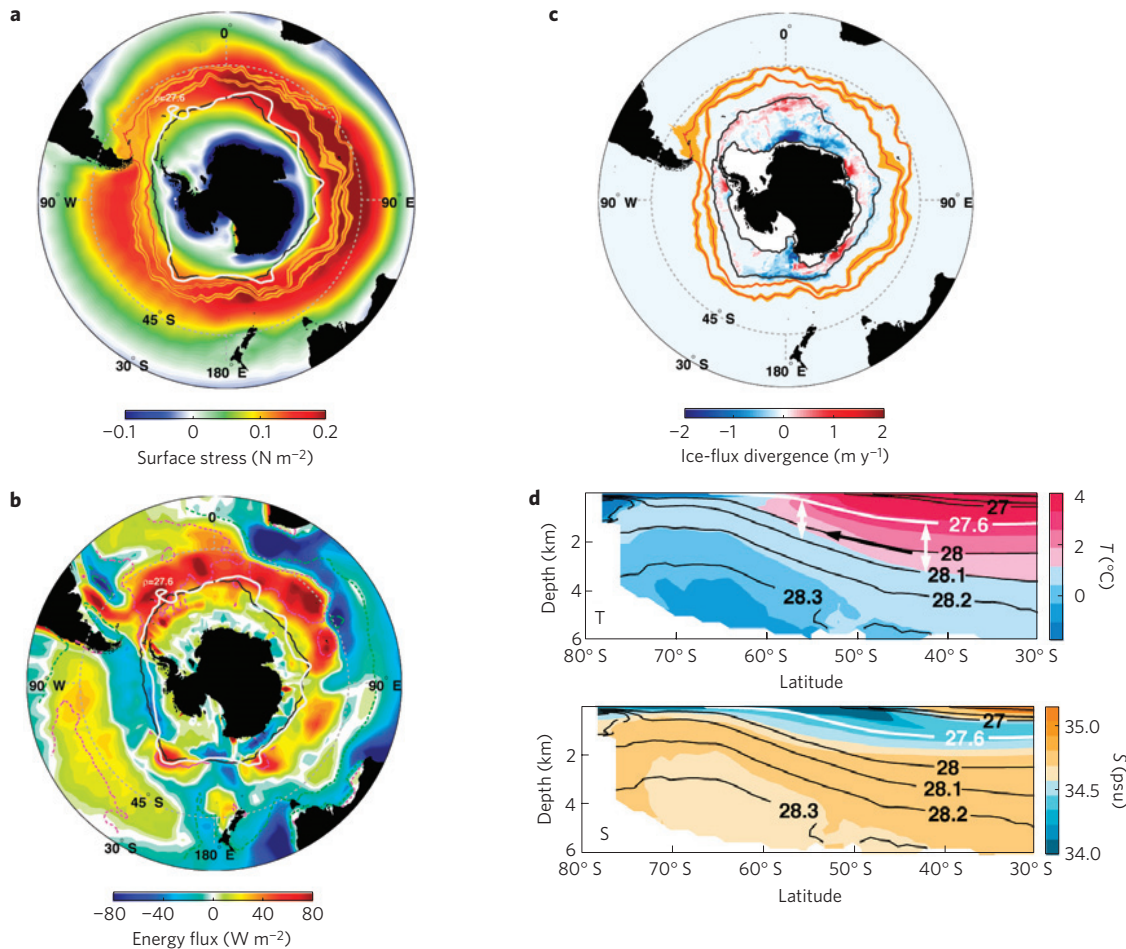
Figure 4 | Air–sea fluxes over the Southern Ocean. a, The mean zonal wind stress, τ_x (see colour scale) for the period 1980–2000 from the National Centers for Environmental Prediction (NCEP) reanalysis. Subantarctic and polar fronts are marked in orange as in Fig. 2. The winter ice edge is marked by the black line and the 27.6 kg m^{-3} outcrop by the white line. **b**, The National Centers for Environmental Predication mean net (radiative + sensible + latent) air–sea heat flux for the same period, including contributions from evaporation and precipitation expressed as a pseudo-heat flux. Blue indicates regions where the heat flux is out of the ocean, and yellow–orange represents regions where it is directed into the ocean. As in **a**, the black and white lines mark the position of the winter ice edge and the 27.6 kg m^{-3} outcrop. **c**, An estimate of the freshwater flux contribution from sea-ice manufacture and export: red shading indicates buoyancy gain by the ocean and blue shading indicates buoyancy loss. The position of the summer and winter sea-ice edge is marked in black. The area within the summer ice edge is shaded in white. The subantarctic and polar front positions are again marked in orange. Data sources and methods are described by Li and colleagues[101]. **d**, Circumpolar zonal average of temperature (T) and salinity (S) (scales on right) from the CARS2209 atlas (courtesy of the Commonwealth Scientific and Industrial Research Organisation) with density contoured in black. The vertical white lines indicate the thickness of the density layers. The black arrow marks the sense of the eddy-induced upwelling.

departures from that average: ψ is a stream function (with units of m^3 s^{-1} that is in Sverdrups, Sv) representing the flow in the meridional plane. The residual flow is of central importance because it is this flow, rather than the Eulerian mean, that advects tracer properties in a turbulent ocean.

The dynamical processes at work are shown in the numerical results presented in Fig. 5 from a very high-resolution process model of a portion of the ACC (ref. 45). The wind induces a pattern of upwelling and downwelling, an analogue of the Deacon cell represented by $\overline{\psi}$ in the diagram, tilting up density surfaces. This is largely balanced by the circulation associated with eddies, ψ^*, acting to return them to the horizontal. Note that both $\overline{\psi}$ and ψ^* cross mean density surfaces. However, the upwelling branch of residual mean flow, ψ_{res}, is directed along mean density surfaces and not associated with elevated levels of diapycnal mixing. A tracer released into the flow disperses along neutral density surfaces, as seen in Fig. 5. The upwelling feeds an upper cell and a lower cell, similar to the data inversion shown in Fig. 3 and schematized in Fig. 1. These cells are associated with air–sea density fluxes (indicated at the top

of Fig. 5) with a cooling (blue), warming (red), cooling pattern evident in the data (broadly reminiscent of Fig. 4b,c).

The dynamical balances in the model and in the Southern Ocean can be described in terms of a streamwise force balance for a density layer of mean thickness $\overline{h}$ (ref. 46):

$$-\rho_0 f \overline{vh} = \overline{F}_{eddy} + \overline{F}_{wind} - \frac{\Delta P}{L_x} \quad (2)$$

expressing a balance between: the Coriolis force; eddy form-drag forces related to the isopycnal eddy flux of potential vorticity $\overline{F}_{eddy} = \rho_0 \overline{h}^2 \overline{v'Q'}$, where ρ_0 is the mean density, $Q = (f + \zeta)/h$ is the Ertel potential vorticity, f is the planetary vorticity owing to Earth's rotation (the Coriolis parameter) and ζ is the vertical component of the relative vorticity; the driving force owing to the prevailing winds $\overline{F}_{wind}$; and the (back) pressure gradient force, $\Delta P/L_x$, owing to the intersection of the layer with bottom ridges and/or continental margins[47,48], where L_x is the distance around Antarctica. The balance in equation (2) holds as long as the Rossby number of the
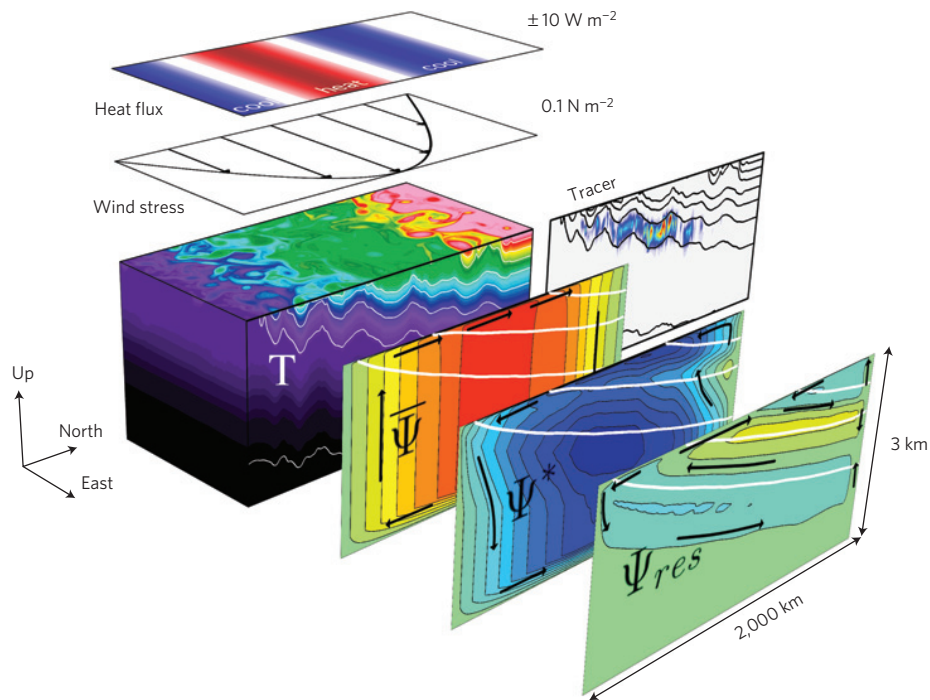
Figure 5 | Idealized simulations of the ACC. Results from numerical simulations of an eddying re-entrant channel showing the wind and surface heat fluxes driving the channel flow (overlaid above); an instantaneous three-dimensional snapshot of the model's temperature field T (here coincident with density $\rho = \rho(T)$), with two density surfaces picked out in white, undulating in concert with the mesoscale eddy field; and time-mean overturning cells $\overline{\psi}$, ψ^* and ψ_{res} (computed as defined in equation (1)) with time-mean density surfaces plotted in white. Also shown is an instantaneous section of tracer released into the flow. Antarctica is imagined to be on the left. The model is the MITgcm run at a horizontal resolution of 4 km over a 1,000 km by 3,000 km domain. The cooling (blue), warming (red), cooling pattern of air–sea fluxes, on moving out from Antarctica, are arranged to be reminiscent of Fig. 4b, and lead to the particular pattern of upper and lower residual overturning cells seen in ψ_{res}. More details can be found from Abernathey and colleagues[45].

large-scale circulation is small, a condition well satisfied in the ACC system. The meridional mass flux, $\overline{vh}$, equation (1), is driven by the three terms appearing on the right-hand side of equation (2). In mid-latitudes, winds and pressure forces dominate the budget. But in the upper levels of the ACC where zonal flow does not intersect with bottom topography ($\Delta P = 0$), the eddy-forcing term enters at leading order, balancing in part the wind forcing and resulting in a meridional residual flow.

Using the momentum budget in equation (2), we can now infer the MOC and its upwelling pattern in terms of hydrographic measurements of the density field. Hypothesizing that eddies mix potential vorticity[49], v_{res} is an inevitable and rather general consequence of eddies acting on the geometry of the isopycnal layers to smooth out thickness gradients. Beneath the direct influence of the wind and above topographic ridges where $\overline{F}_{wind}$ and ΔP are zero, equation (2) implies that:

$$\overline{vh} = -\frac{\overline{h}^2}{f}\overline{v'Q'} = \frac{\overline{h}^2}{f}K\frac{\partial \overline{Q}}{\partial y} = -K\left(\frac{\partial \overline{h}}{\partial y} - \frac{\overline{h}}{f}\beta\right) \simeq -K\frac{\partial \overline{h}}{\partial y} \quad (3)$$

where the mean Q gradient is evaluated on a density surface of mean thickness $\overline{h}$, K is an eddy diffusivity acting along density surfaces, y is a coordinate increasing northwards and β is the meridional gradient of f. In the ACC, meridional gradients in $\overline{Q}$ are dominated by thickness gradients[50] and so to a good approximation the residual flux is directed from regions where density layers are thick to regions where they are thin. In Fig. 4d we present a zonal average density section around Antarctica, with $\overline{T}$ and $\overline{S}$ superimposed. The thickness gradient is evident by comparing the vertical extent of the white arrows drawn at different latitudes. The thickening of layers moving northwards implies, from equation (3), a southward and upward volume transport—a thickness diffusion[51]—directed along

sloping isopycnals, as marked by the black arrow in Fig. 4d, just as inferred from observations (Fig. 3) and evident in the eddying model (Fig. 5). This is the primary mechanism, we believe, returning water from mid-depth to the surface. The implied volume flux is of magnitude $L_x K \partial \overline{h}/\partial y$ where $L_x \simeq 20,000$ km, (assuming the eddies are acting all the way around the ACC), $\partial \overline{h}/\partial y$ is the meridional thickness gradient, typically 500 m in 1,000 km, and K measures the vigour with which the eddy field smooths out thickness gradients. If $K = 1,000$ m^2 s^{-1}, typical of eddy diffusivities at mid-depth, such gradients imply a residual southward and upward water mass transport of roughly 10 Sv (refs 26,28), much less than the Ekman transport but comparable to the strength of the upwelling branch observed in Fig. 3. So, what are the implications of this upwelling branch for climate?

The Southern Ocean in climate and climate change

The North Atlantic MOC has long been considered a major control of the climate system[52]. However, along with the growing realization of the importance of the upwelling branch of the MOC, the Southern Ocean is now taking centre stage in discussions of processes that drive modern and ancient climate variability[53].

Proxy data show that for a period of at least the past 800,000 years, Antarctic temperatures have covaried with atmospheric CO_2, although the relationship may not be causal. Moreover, it seems likely that marine processes operating in the Southern Ocean may have played a central role in setting atmospheric CO_2 levels on glacial–interglacial timescales[54]. Biogeochemical box models indicate the strong sensitivity of atmospheric CO_2 levels to perturbations of high-latitude surface ocean processes[55,56]. The precise mechanisms are an active area of research. Many hypotheses invoke variations in the efficiency of communication between the carbon reservoir of the deep ocean and the surface. Accumulation of

Box 1 | The MOC of the world ocean.

Broecker[95,96] put forward an ocean circulation schematic in which polar sinking is balanced by upwelling from depth through the thermocline of the North Pacific, as sketched in his famous conveyor belt analogy, inspired from earlier descriptions[97]. The neglect of a role for the Southern Ocean was subsequently addressed[74,98,99]. Here we have revised and updated Broecker's famous conveyor to draw out the asymmetry among the Atlantic, Pacific and Indian basins and between the Northern and Southern hemispheres, and to emphasize the central role of Southern Ocean upwelling. The upper cell of ocean circulation is fed predominantly by broad upwelling across surfaces of equal density at mid-depths, distributed over the main ocean basins (rising blue–green–yellow arrows). Upwelling to the ocean surface occurs mainly around Antarctica along surfaces of equal density (rising yellow–red arrows) with wind and eddy processes playing a central role. Much of this upwelled water is converted into intermediate-depth mode waters and, after entering various thermocline layers, it eventually resupplies the upper branch of the global cell in the Atlantic with relatively warmer waters.

In the northern North Atlantic, warm water is cooled in the subpolar gyre and eventually becomes dense enough to sink under the thermocline in the polar seas and Labrador Sea convection regions (blue arrows). The dense water formed by convection in the Atlantic flows southwards in the deep branch of the upper cell (green arrow), before joining the ACC system. Below that, in turn, is the even denser bottom water that spreads from Antarctica and feeds the upwelling branch of the lower cell. Antarctic regions where water sinks to great depth are indicated in the Weddell and Ross seas around Antarctica and the Labrador and Greenland–Iceland seas in the northern North Atlantic. (Figure 1 represents a zonal average view of this complex pattern). To construct such a diagram, much of the richness of the ocean's three-dimensional circulation structure has to be ignored, and only an overall, idealized representation of the cells can be shown. Cooler colours indicate denser water masses, ranging from warmer mode and thermocline waters in red to bottom waters in blue.

The new diagram builds on previous ones[99], links old and new ideas and brings the Southern Ocean to the forefront of the MOC.
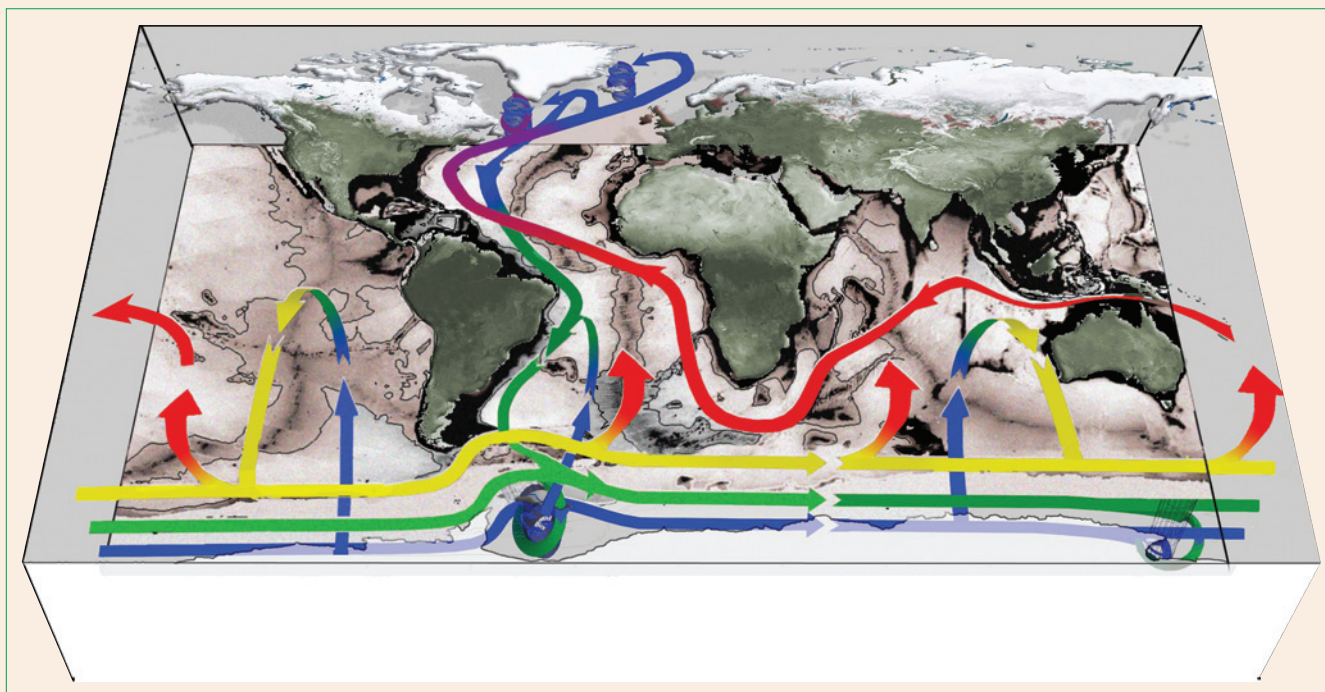
CO_2 in the deep, cold, sluggish ocean occurs during glacial periods when, it seems, the ocean was more salty and more stratified[57]. Communication between the interior ocean and the surface may have been less efficient than today, mainly as a result of reduced residual upwelling rates but also suppressed mixing. Release of abyssal CO_2 into the atmosphere may be indicative of increased exchange between the deep and the surface, and could have contributed to, for example, the transition out of the last ice age[58,59].

Communication between the deep and surface in the modern ocean is governed by the upwelling branch of the MOC, but how it operated in glacial periods is unclear. Proxy data indicate that upwelling patterns may have been very different from today. For example, the winter sea-ice edge in glacial times was probably at the position of today's polar front, and the summer ice edge close to where the winter ice edge is today[60,61].

A number of mechanisms have been proposed in which the upwelling branch of the Southern Ocean plays a central role in glacial cycles, elements of which may all have had an impact. First,

sea-ice cover[62]. Increased sea-ice cover in glacial times could have reduced the outgassing of CO_2 from the upwelling branch of the MOC, thereby reducing the concentration of atmospheric CO_2. Second, the bipolar seesaw[63]. Changes in Southern Hemisphere climate may be caused by a cessation of the MOC in the Northern Hemisphere, induced by freshwater release owing to glacial melt in the North Atlantic/Arctic. Heat remains in the Southern Hemisphere owing to reduced northward heat transport, melting back sea ice and allowing winds to drive air–sea exchange more efficiently between deep and surface waters. Third, Southern Hemisphere westerly wind shifts[59,64,65]. In cold climates the surface westerlies may have been significantly equatorward (perhaps ~10°) of their present position and so not aligned with Drake Passage. Thus the wind stress may have been largely balanced by the pressure gradient term in equation (2) implying reduced residual meridional flow and upwelling rates. As the climate warmed, the surface westerlies may have shifted southwards towards their present location, turning on the upwelling branch of the MOC

177

and enhancing communication between the abyss and the surface, releasing CO_2 to the atmosphere and so accelerating the warming. Fourth, a reorganization of air–sea density fluxes in glacial times[66]. The much colder atmospheric temperatures of glacial times and/or the reduced hydrological forcing could have altered the pattern of surface-density fluxes over the Southern Ocean, resulting in an increase in eddy fluxes, further compensating the Ekman-driven Deacon cell and resulting in a decrease in residual upwelling.

The Southern Ocean and its upwelling MOC branch are also central to our understanding of how the climate is responding to anthropogenic forcing. In today's climate the dominant mode of climate and atmospheric variability in the extratropical Southern Hemisphere is the Southern Annular Mode[67]. In recent decades the Southern Annular Mode has shown a marked upward trend, the probable result of a combination of ozone depletion and anthropogenic global warming[68,69]. Strengthening of the Southern Annular Mode and associated surface wind stress have been invoked to postulate enhancement in the strength of the upwelling branch of the MOC, and increases in the slope of density surfaces and eddy heat fluxes of the ACC (refs 70,71). Enhanced communication of the interior ocean with the surface could have marked effects on Earth's climate through changes in rates of heat and carbon sequestration as well as consequences for ice shelves around Antarctica that may be vulnerable to enhanced upwelling of warm water from depth[72,73]. The stratification of the Southern Ocean is also delicately poised and may be particularly sensitive to changes in the freshwater balance[74].

The links between the upwelling of deep water in the Southern Ocean and the Southern Hemisphere westerly winds and consequences for climate have been examined in observations and models[75]. Although changes in the slope of density surfaces in the ACC cannot yet be detected[76], ocean observations do indicate a freshening of Antarctic Intermediate Water[77,78] and a substantial warming of the Southern Ocean at all depths[79,80], which may be linked to atmospheric forcing[81]. Modelling studies and theory, however, indicate that eddy transport in the ACC (ψ^*—see equation (1)) can readily compensate for changes in Ekman transport ($\overline{\psi}$) leading to little change in the strength of the MOC (ψ_{res}) (refs 45,82–84).

The Southern Ocean is also the primary region where anthropogenic CO_2 enters the ocean from the atmosphere[85–87] and is subsequently incorporated into mode and intermediate waters[88–90]. Observations indicate that the outgassing of natural CO_2 from the interior ocean has increased in the past twenty years[91], offsetting the anthropogenic source. Some studies argue that this may be linked to an increase in the westerly winds blowing over the Southern Ocean[92], whereas other studies question whether increased outgassing is occurring[93]. The net (natural + anthropogenic) CO_2 flux depends on the strength of the wind, upwelling and the mixed-layer cycle of carbon and nutrients and is thus directly related to the dynamics of the MOC's residual upwelling branch. Climate models predict that the wind stress over the Southern Ocean is likely to increase and shift slightly polewards[94] under global warming and ozone depletion, with surface waters becoming warmer and lighter, although there remains some uncertainty[68]. The consequence of this increase may be a reduction in the efficiency of the Southern Ocean sink of CO_2 and thus a possibly higher level of stabilization of atmospheric CO_2 on a multicentury timescale.

Update of the global overturning circulation

In this Review we have drawn explicit attention to the importance of the Southern Ocean upwelling branch of the MOC circulation in the climate system. This upwelling branch roughly balances the North Atlantic downwelling branch and, because it is much more distributed in space, acts to connect the vast reservoirs of heat and carbon below the Southern Ocean mixed layer with the surface. As a result, the upwelling branch is now thought to be a

significant player in climate. Its dynamics have been brought into focus through full consideration of the central role of eddies in the momentum and tracer balances.

We conclude with a revised overturning schematic (Box 1) that represents a significant update compared with Broecker's iconic conveyor belt[95,96] and appropriately acknowledges the role of the Southern Ocean upwelling branch. It is based on the quantitative results and qualitative ideas that have been developed over the past decades, and draws on the many individual studies that were made as part of larger experimental programmes, such as the World Ocean Circulation Experiment. The notion of deep water rising towards the surface to replace surface water blown north, or that of dense water sinking towards the bottom, in the Southern Ocean is not new[100]. But now we have a global quantification of flows and property fluxes, a compelling dynamical theory put forth in explanation and a growing realization of the importance of the upwelling system in global climate.

The emerging link between upwelling and mesoscale eddy fluxes places a large burden on climate models as the—relatively small-scale—eddy fluxes are computationally difficult to obtain and their parameterizations may not always be faithful, especially in a changing climate. Yet many questions of primary importance are directly linked to the influence of eddy fluxes. Whether rising deep water will bring natural CO_2 to the surface and overwhelm the Southern Ocean anthropogenic sink, whether changing winds will accelerate the melting of Antarctic sea ice and glaciers, or change the strength of the ACC, and how the Southern Ocean operated in past climates cannot be resolved without a fundamental understanding of Southern Ocean upwelling.

Deep-water formation in the Northern Hemisphere has long received much attention as the axis of climate change. The upwelling branch in the Southern Ocean is now being recognized as a vital component of our climate system and an equally important agent of global change.

References

1. Stommel, H. The abyssal circulation. Letter to the editors. *Deep-Sea Res.* **5,** 80–82 (1958).
2. Hughes, G. O. & Griffiths, R. W. A simple convective model of the global overturning circulation, including effects of entrainment into sinking regions. *Ocean Model.* **12,** 46–79 (2006).
3. Marshall, J. & Schott, F. Open ocean deep convection: Observations, models and theory. *Rev. Geophys.* **37,** 1–64 (1999).
4. Munk, W. Abyssal recipes. *Deep-Sea Res.* **13,** 707–730 (1966).
5. Munk, W. & Wunsch, C. Abyssal recipes II: Energetics of tidal and wind mixing. *Deep-Sea Res.* **145,** 1977–2010 (1998).
6. Toole, J. M. The Brazil Basin tracer release experiment. *Int. WOCE Newsl.* **28,** 25–28 (1997).
7. Kunze, E., Firing, E., Hummon, J., Chereskin, T. & Thurnherr, A. M. Global abyssal mixing inferred from lowered adcp shear and ctd strain profiles. *J. Phys. Oceanogr.* **36,** 1553–1576 (2006).
8. Ledwell, J. R., Watson, A. J. & Law, C. S. Mixing of a tracer in the pycnocline. *J. Geophys. Res.* **103,** 21499–21529 (1998).
9. Ledwell, J. R., St Laurent, L. C., Girton, J. B. & Toole, J. M. Diapycnal mixing in the Antarctic circumpolar current. *J. Phys. Oceanogr.* **41,** 241–246 (2011).
10. Sverdrup, H. U. On vertical circulation in the ocean due to the action of the wind with application to conditions within the Antarctic Circumpolar Current. *Discov. Rep.* **VII,** 139–170 (1933).
11. Döös, K. & Webb, D. J. The deacon cell and the other meridional cells of the southern ocean. *J. Phys. Oceanogr.* **24,** 429–442 (1994).
12. Toggweiler, J. R. & Samuels, B. Effect of Drake Passage on the global thermohaline circulation. *Deep-Sea Res. I* **42,** 477–500 (1995).
13. Toggweiler, J. R. & Samuels, B. On the ocean's large-scale circulation near the limit of no vertical mixing. *J. Phys. Oceanogr.* **28,** 1832–1852 (1998).
14. Webb, D. J. & Suginohara, N. in *Ocean Circulation and Climate* (eds Siedler, G., Church, J. & Gould, J.) Chapter 4.2, 205–214 (Int. Geophys. Ser., vol. 77, Academic, 2001).
15. Deacon, G. E. R. The hydrology of the Southern Ocean. *Discov. Rep.* **15,** 1–124 (1937).

16. Wyrtki, K. The Antarctic circumpolar current and the Antarctic polar front. *Dtsch. Hydrogr. Z.* **13,** 153–174 (1960).

17. Jacobs, S. & Georgi, D. T. Observations on the southwest Indian/Antarctic Ocean. *Deep-Sea Res.* **24,** 43–84 (1977).

18. McCartney, M. S. in *A Voyage of Discovery: George Deacon 70th Anniversary Volume* (ed. Angel, M. V.) 103–119 (Supplement to Deep-Sea Research, vol. 24, Pergamon, 1977).

19. Whitworth, T. III, Orsi, A. H., Kim, S-J., Nowlin, W. D. Jr & Locarnini, R. A. in *Ocean, Ice, and Atmosphere: Interactions at the Antarctic Continental Margin* Vol. 75 (eds Jacobs, S. S. & Weiss, R. F.) (Antarctic Research Series, American Geophysical Union, 1998).

20. Nowlin, W. D. & Klinck, J. M. The physics of the Antarctic Circumpolar Current. *Rev. Geophys. Space Phys.* **24,** 469–491 (1986).

21. Orsi, A. H., Whitworth, T.W. III & Nowlin, W. D. Jr On the meridional extent and fronts of the Antarctic Circumpolar Current. *Deep-Sea Res.* **42,** 641–673 (1995).

22. Pollard, R. T., Lucas, M. I. & Read, J. F. Physical controls on biogeochemical zonation in the Southern Ocean. *Deep-Sea Res. II* **49,** 3289–3305 (2002).

23. Sloyan, B. M. & Rintoul, S. R. The Southern Ocean limb of the global deep overturning circulation. *J. Phys. Oceanogr.* **31,** 143–173 (2001).

24. Talley, L. D., Reid, J. L. & Robbins, P. E. Data-based meridional overturning streamfunctions for the global ocean. *J. Clim.* **16,** 3213–3226 (2003).

25. Lumpkin, R. & Speer, K. Global ocean meridional overturning. *J. Phys. Oceanogr.* **37,** 2550–2562 (2007).

26. Speer, K., Rintoul, S. R. & Sloyan, B. The diabatic Deacon Cell. *J. Phys. Oceanogr.* **30,** 3212–3222 (2000).

27. Karsten, R. & Marshall, J. Inferring the residual circulation of the Antarctic circulation current from observations using dynamical theory. *J. Phys. Oceanogr.* **32,** 3315–3327 (2002).

28. Marshall, J., Shuckburgh, E., Jones, H. & Hill, C. Estimates and implications of near-surface eddy diffusivities deduced by trace transport in the southern ocean. *J. Phys. Oceanogr.* **36,** 1806–1821 (2006).

29. Zika, J. D., Sloyan, B. M. & McDougall, T. J. Diagnosing the Southern Ocean overturning from tracer fields. *J. Phys. Oceanogr.* **39,** 2926–2940 (2009).

30. Jenkins, A. & Jacobs, S. Circulation and melting beneath George VI Ice Shelf, Antarctica. *J. Geophys. Res.* **113,** C04013 (2008).

31. Warren, B., LaCasce, J. & Robbins, P. A. On the obscurantist physics of 'form drag' in theorizing about the Circumpolar Current. *J. Phys. Oceanogr.* **26,** 2297–2301 (1996).

32. Toole, J. M. Sea ice, winter convection, and the temperature minimum layer in the Southern Ocean. *J. Geophys. Res.* **86,** 8037–8047 (1981).

33. Rintoul, S., Hughes, C. & Olbers, D. in *Ocean Circulation and Climate* (eds Siedler, G., Church, J. & Gould, J.) Chapter 4.6, 271–302 (Int. Geophys. Ser., vol. 77, Academic, 2001).

34. Gill, A. E., Green, J. S. A. & Simmons, A. J. Energy partition in the large-scale ocean circulation and the production of midocean eddies. *Deep-Sea Res.* **21,** 499–528 (1974).

35. Marshall, J. & Radko, T. Residual mean solutions for the Antarctic Circumpolar Current and its associated overturning circulation. *J. Phys. Oceanogr.* **33,** 2341–2354 (2003).

36. Wunsch, C. The work done by the wind on the oceanic general circulation. *J. Phys Oceanogr.* **28,** 2332–2340 (1998).

37. McWilliams, J. C., Holland, W. R. & Chow, J. S. A description of numerical Antarctic Circumpolar Currents. *Dyn. Atmos. Oceans* **2,** 213–291 (1978).

38. Marshall, J. On the parameterization of geostrophic eddies in the ocean. *J. Phys. Oceanogr.* **11,** 1257–1271 (1981).

39. deSzoeke, R. A. & Levine, M. D. The advective flux of heat by mean geostrophic motions in the Southern Ocean. *Deep-Sea Res. A* **28,** 1057–1085 (1981).

40. Johnson, G. C. & Bryden, H. L. On the size of the Antarctic Circumpolar Current. *Deep-Sea Res.* **36,** 39–53 (1989).

41. Gnanadesikan, S. A simple predictive model for the structure of the oceanic pycnocline. *Science* **283,** 2077–2079 (1999).

42. Olbers, D. & Visbeck, M. A model of the zonally-averaged stratification and overturning in the southern ocean. *J. Phys. Oceanogr.* **35,** 1190–1205 (2005).

43. Hallberg, R. & Gnanadesikan, A. The role of eddies in determining the structure and response of the wind-driven Southern Hemisphere overturning: results from the modeling eddies in the souther ocean (meso) project. *J. Phys. Oceanogr.* **36,** 2232–2252 (2006).

44. Danabasoglu, G. & McWilliams, J. C. Sensitivity of the global ocean circulation to parameterization of mesoscale tracer transports. *J. Clim.* **8,** 2967–2980 (1995).

45. Abernathey, R., Marshall, J. & Ferreira, D. Dependence of southern ocean overturning on wind stress. *J. Phys. Oceanogr.* **41,** 2261–2278 (2011).

46. Marshall, D. Subduction of water masses in an eddying ocean. *J. Mar. Res.* **55,** 201–222 (1997).

47. Munk, W. H. & Palmen, E. Note on the dynamics of the Antarctic Circumpolar Current. *Tellus* **3,** 53–55 (1951).

48. Gille, S. The Southern Ocean momentum balance: Evidence for topographic effects from numerical model output and altimeter data. *J. Phys. Oceanogr.* **27,** 2219–2231 (1997).

49. Rhines, P. B. & Young, W. R. Homogenization of potential vorticity in planetary gyres. *J. Fluid Mech.* **122,** 347–367 (1982).

50. Marshall, J. C., Olbers, D., Wolf-Gladrow, D. & Ross, H. Potential vorticity constraints on the hydrography and transport of the southern oceans. *J. Phys. Oceanogr.* **23,** 465–487 (1993).

51. Gent, P. R. & McWilliams, J. C. Isopycnal mixing in ocean circulation models. *J. Phys. Oceanogr.* **20,** 150–155 (1990).

52. Alley, R. B. Abrupt climate change. *Science* **299,** 2005–2010 (2003).

53. Huybers, P. & Wunsch, C. Paleophysical oceanography with an emphasis on transport rates. *Annu. Rev. Marine Sci.* **2,** 1–34 (2010).

54. Sigman, D. & Boyle, E. Glacial/interglacial variations in atmospheric carbon dioxide. *Nature* **407,** 859–869 (2000).

55. Sarmiento, J. L. & Toggweiler, J. R. A new model for the role of the oceans in determining atmospheric CO_2. *Nature* **308,** 621–624 (1984).

56. Knox, F. & McElroy, M. B. Changes in atmospheric CO_2: Influence of the marine biota at high latitude. *J. Geophys. Res.* **89,** 4629–4637 (1984).

57. Adkins, J. F., McIntyre, K. & Schrag, D. P. The salinity, temperature and $\delta^{18}O$ of the glacial deep ocean. *Science* **298,** 1769–1773 (2002).

58. Skinner, L. C., Fallon, S., Waelbroeck, C., Michel, E. & Barker, S. Ventilation of the deep southern ocean and deglacial CO_2 Rise. *Science* **328,** 1147–1151 (2010).

59. Anderson, R. F. *et al.* Wind-driven upwelling in the southern ocean and the deglacial rise in atmospheric CO_2. *Science* **323,** 1443–1448 (2009).

60. Crosta, X., Pichon, J. J. & Burckle, L. H. Reappraisal of seasonal Antarctic sea-ice extent at the last glacial maximum. *Geophys. Res. Lett.* **25,** 2703–2706 (1998).

61. Gersonde, R., Crosta, X., Abelmann, A. & Armand, L. Sea-surface temperature and sea ice distribution of the Southern Ocean at the EPILOG Last Glacial Maximum—a circum-Antarctic view based on siliceous microfossil records. *Quat. Sci. Rev.* **24,** 869–896 (2005).

62. Stephens, B. & Keeling, R. The influence of Antarctic sea ice on glacial–interglacial CO_2 variations. *Nature* **404,** 171–174 (2000).

63. Stocker, T. F. The sea saw effect. *Science* **282,** 61–62 (1998).

64. Toggweiler, J. R., Russell, J. L. & Carson, S. R. Midlatitude westerlies, atmospheric CO_2, and climate change during the ice ages. *Paleoceanography* **21,** PA2005 (2006).

65. Toggweiler, J. R. & Russell, J. Ocean circulation in a warming climate. *Nature* **451,** 286–288 (2008).

66. Watson, A. J. & Naveria Garabato, A. C. The role of Southern Ocean mixing and upwelling in glacial–interglacial CO_2 change. *Tellus B* **58,** 73–87 (2006).

67. Thompson, D. W. J. & Wallace, J. M. Annular modes in the extratropical circulation. Part I: Month-to-month variability. *J. Clim.* **13,** 1000–1016 (2000).

68. Thompson, D. W. J. & Solomon, S. Interpretation of recent Southern Hemisphere climate change. *Science* **296,** 895–899 (2002).

69. Thompson, D. W. J. *et al.* Signatures of the Antarctic ozone hole in Southern Hemisphere surface climate change. *Nature Geosci.* **4,** 741–749 (2011).

70. Hall, A. & Visbeck, M. Synchronous variability in the Southern Hemisphere atmosphere, sea ice, and ocean resulting from the annular mode. *J. Clim.* **15,** 3043–3057 (2002).

71. Hogg, A., Meredith, M. P., Blundell, J. R. & Wilson, C. Eddy heat flux in the Southern Ocean: Response to variable wind forcing. *J. Clim.* **21,** 608–620 (2008).

72. Martinson, D. G., Stammerjohn, S. E., Ianuzzi, R. A., Smith, R. C. & Vernet, M. Western Antarctic Peninsula physical oceanography and spatio-temporal variability. *Deep-Sea Res. II* **55,** 1964–1987 (2008).

73. Holland, P. R., Jenkins, A. & Holland, D. M. Ice and ocean processes in the Bellingshausen Sea, Antarctica. *J. Geophys. Res.* **115,** C05020 (2010).

74. Gordon, A. *Lamont–Doherty Geological Observatory 1990 & 1991 Report* 44–51 (Lamont-Doherty Geological Observatory of Columbia Univ., 1991).

75. Russell, J. L., Dixon, K. W., Gnanadesikan, A., Stouffer, R. J. & Toggweiler, J. R. The Southern Hemisphere westerlies in a warming world: Propping open the door to the deep ocean. *J. Clim.* **19,** 6382–6390 (2006).

76. Boening, C. W., Dispert, A. & Visbeck, M. The response of the Antarctic Circumpolar Current to recent climate change. *Nature Geosci.* **1,** 864–869 (2008).

77. Wong, A. P. S., Bindoff, N. L. & Church, J. A. Large-scale freshening of intermediate waters in the Pacific and Indian oceans. *Nature* **400,** 440–443 (1999).

78. Durack, P. J. & Wijffels, S. E. Fifty-year trends in global ocean salinities and their relationship to broad-scale warming. *J. Clim.* **23,** 4342–4362 (2010).

79. Gille, S. Decadal-scale temperature trends in the Southern Hemisphere ocean. *J. Clim.* **21,** 2749–2765 (2008).

80. Purkey, S. G. & Johnson, G. C. Warming of global abyssal and deep southern ocean waters between the 1990s and 2000s: Contributions to global heat and sea level rise budgets. *J. Clim.* **23,** 6336–6351 (2010).

81. Fyfe, J. C., Saenko, O. A., Zickfeld, K., Eby, M. & Weaver, A. J. The role of poleward-intensifying winds on Southern Ocean warming. *J. Clim.* **20,** 5391–5400 (2007).

82. Henning, C. C. & Vallis, G. K. The effects of mesoscale eddies on the stratification and transport of an ocean with a circumpolar channel. *J. Phys. Oceanogr.* **35,** 880–897 (2005).

83. Hallberg, R. & Gnanadesikan, A. The role of eddies in determining the structure and response of the wind-driven Southern Hemisphere overturning: Results from the modeling eddies in the southern ocean (meso) project. *J. Phys. Oceanogr.* **36,** 2232–2252 (2006).

84. Treguier, A. M., Le Sommer, J., Molines, J. M. & de Cuevas, B. Response of the Southern Ocean to the southern annular mode: Interannual variability and multidecadal trend. *J. Phys. Oceanogr.* **40,** 1659–1668 (2010).

85. Caldeira, K. & Duffy, P. B. The role of the Southern Ocean in uptake and storage of anthropogenic carbon dioxide. *Science* **287,** 620–622 (2000).

86. Sabine, C. L. *et al.* The oceanic sink for anthropogenic CO_2. *Science* **305,** 367–371 (2004).

87. Lenton, A. & Matear, R. J. Role of the Southern Annular Mode (SAM) in Southern Ocean CO_2 uptake. *Glob. Biogeochem. Cycles* **21,** GB2016 (2007).

88. Sarmiento, J. L., Gruber, N., Brzezinski, M. A. & Dunne, J. P. High-latitude controls of thermocline nutrients and low latitude biological productivity. *Nature* **427,** 56–60 (2004).

89. Mignone, B. K., Gnanadesikan, A, Sarmiento, J. L. & Slater, R. D. Central role of Southern Hemisphere winds and eddies in modulating the anthropogenic carbon. *Geophys. Res. Lett.* **33,** L01604 (2006).

90. Ito, T., Marshall, J. & Follows, M. What controls the uptake of transient tracers in the Southern Ocean? *Glob. Biogeochem. Cycles* **18,** GB2021 (2004).

91. le Quéré, C., Rodenbeck, C. & Buitenhuis, E. T. Saturation of the Southern Ocean CO_2 sink due to recent climate change. *Science* **316,** 1735–1738 (2007).

92. Lovenduski, N. S., Gruber, N. & Doney, S. C. Toward a mechanistic understanding of the decadal trends in the Southern Ocean carbon sink. *Glob. Biogeochem. Cycles* **22,** GB3016 (2008).

93. Zickfeld, K., Fyfe, J. C., Eby, M. & Weaver, A. J. Comment on 'Saturation of the Southern Ocean CO_2 sink due to recent climate change'. *Science* **319,** 570–571 (2008).

94. Meehl, G. A. *et al.* in *IPCC Climate Change: The Physical Science Basis* (eds Solomon, S. *et al.*) 747–845 (Cambridge Univ. Press, 2007).

95. Broecker, W. S. The biggest chill. *Nat. Hist. Mag.* **97,** 74–82 (1987).

96. Broecker, W. S. The great ocean conveyor. *Oceanography* **4,** 79–89 (1991).

97. Gordon, A. L. Interocean exchange of thermocline water. *J. Geophys. Res.* **91,** 5037–5046 (1986).

98. Schmitz, W. J. Jr *On the World Ocean Circulation, 1 & II, Tech. Rep. WHOI-96-O3&O8* (Woods Hole Oceanographic Institute, 1996).

99. Richardson, P. L. On the history of meridional overturning circulation schematic diagrams. *Prog. Oceanogra.* **76,** 466–486 (2008).

100. Sverdrup, H. U., Johnson, M. W. & Fleming, R. H. *The Oceans, their Physics, Chemistry, and General Biology* (Prentice Hall, 1942).

101. Ren, L., Speer, K. & Chassignet, E. P. The mixed layer salinity budget and sea ice in the Southern Ocean. *J. Geophys. Res.* **116,** C08031 (2011).

Additional information

The authors declare no competing financial interests. Reprints and permissions information is available online at www.nature.com/reprints. Correspondence and requests for materials should be addressed to J.M.